Pure ultraviolet emission from ZnO nanowire-based *p-n* heterostructures

Xing-Yu Liu,[1,2] Chong-Xin Shan,[1,*] Chen Jiao,[1,2] Shuang-Peng Wang,[1] Hai-Feng Zhao,[1] and De-Zhen Shen[1]

[1]*State Key Laboratory of Luminescence and Applications, Changchun Institute of Optics, Fine Mechanics and Physics, Chinese Academy of Sciences, No. 3888 Dongnanhu Road, Changchun 130033, China*

[2]*University of Chinese Academy of Sciences, Beijing 100049, China*

**Corresponding author: shancx@ciomp.ac.cn*

Received November 5, 2013; revised December 8, 2013; accepted December 11, 2013; posted December 13, 2013 (Doc. ID 200835); published January 20, 2014

Well-aligned ZnO nanowires have been prepared on sapphire substrate, and structural and optical characterizations indicate that the nanowires are of single crystalline and have relatively high luminescent quality. By employing the ZnO nanowires as an active layer, *p*-$Zn_{0.68}Mg_{0.32}O$:N/*n*-ZnO nanowire heterostructure light-emitting devices (LEDs) have been fabricated. The LEDs show pure ultraviolet emission when a forward bias is applied, while the deep-level emission frequently observed in ZnO *p-n* junctions is almost totally invisible. The devices can work continuously for over 27 h under the injection of a current density of 500 mA/cm^2, indicating their good stability.

OCIS codes: (230.5590) Quantum-well, -wire and -dot devices; (160.4670) Optical materials; (230.3670) Light-emitting diodes.

http://dx.doi.org/10.1364/OL.39.000422

The wide direct bandgap and large exciton binding energy make zinc oxide (ZnO) a potential candidate for application in efficient ultraviolet (UV) light-emitting devices (LEDs) and laser diodes [1–11]. Although significant advances have been witnessed in InGaN-based UV and visible LEDs in the past decades [12–16], the step to pursue other high-efficiency exciton-related LEDs and lasers by using ZnO-based technology never stops. There have been a few reports on ZnO based *p-n* junction LEDs [17–22], and in many cases the emission of the LEDs is dominated by a broad emission at around 500 nm, which has been attributed to the deep-level emission of ZnO. The origin for the deep-level emission can be attributed to the structural imperfections in the ZnO active layer due to the relative low crystalline quality of this layer. One of the most wonderful characters of ZnO lies in its rich nanostructure, and it is accepted that self-assembled nanostructures usually have relatively high crystalline quality [4,23–25], so if ZnO nanostructures can be employed as the active layer, the performance of ZnO-based LEDs may be improved. However, although ZnO nanowires have been combined together with other *p* type materials, such as NiO, GaN, etc., to form LEDs [26,27], the emission of such devices is still very poor. One of the major reasons may lie in the poor compatibility between ZnO nanowires and their *p* type counterparts due to the large difference in physical and chemical properties. ZnMgO formed by the alloying of ZnO and MgO has been regarded as one of the most compatible counterparts of ZnO to form heterostructures for their small lattice mismatch and similar bonding state with ZnO. Actually, some groups have fabricated *p*-ZnMgO/*n*-ZnO heterostructures, and some intriguing results have been made from the structures [18,28]. Nevertheless, both reports are focused on ZnO films, while none report on ZnMgO/ZnO heterostructure LEDs employing high-quality ZnO nanowires as the active layer can be found up to date.

In this Letter, vertically aligned ZnO nanowires have been grown, and the nanowires show high crystalline and optical quality. ZnMgO/ZnO *p-n* heterostructures have been fabricated employing the high-quality nanowires as an active layer. The heterostructure LEDs shows pure intense UV emission, while the deep-level emission frequently observed in ZnO *p-n* junctions has been almost totally suppressed.

The ZnO nanowires were grown by a metal-organic chemical vapor deposition (MOCVD) technique using a-plane sapphire as a substrate. The precursors used for the growth of ZnO were diethylzinc and oxygen, and the carrier gas that leads the precursors into the growth chamber was high-purity (9N) nitrogen. Prior to the growth, the substrates were treated at 850°C under 10^{-4} Pa for 60 min to remove the possible absorbed contaminants on the substrate. The substrate temperature was kept at 800°C, and the pressure in the MOCVD chamber at 3000 Pa during the growth process. After the growth, the nanowire samples were loaded into a magnetron sputtering chamber, and there nitrogen-doping ZnMgO layer was deposited onto the nanowires to form the ZnMgO:N/ZnO nanowire heterostructures. For the deposition of the nitrogen-doped ZnMgO layer, a metallic Zn target, and a ceramic $Zn_{0.5}Mg_{0.5}O$ target bound together were employed as the source materials, and nitrogen gas was used as the sputtering ambient. The sputtering was carried out at 550°C for 2 h, and the pressure in the chamber during the sputtering process is around 1 Pa. Finally, a bilayer Ni/Au was deposited onto the ZnMgO layer and an indium layer onto the ZnO nanowires acting as contacts in a thermal evaporation method. The Ni/Au contact was annealed in air ambient at 480°C for 15 min to form an ohmic contact. The morphology of the ZnMgO layer and the ZnO nanowires was characterized using a Hitachi S-4800 field-emission scanning electron microscope (SEM). The structural properties of the ZnO nanowires were assessed by a JEM-2010 transmission electron microscope (TEM) and a Bruke D8 x-ray diffractometer. The electrical properties of the ZnMgO layer were measured by a Lakeshore 7707 Hall measurement system under van der Paul configuration

at room temperature, and the magnetic field used for the Hall measurement is 9000 Gauss. Photoluminescence (PL) studies of the ZnO nanowires were carried out in a spectrometer employing the 325 nm line of a He-Cd laser as the excitation source. Electroluminescence (EL) measurement of the ZnMgO:N/ZnO nanowire heterostructures was carried out in a Hitachi F4500 spectrometer with a continuous current power source.

The morphology of the ZnO nanowires is shown in Fig. 1(a), and one can see from the 30° tilted SEM image that well-aligned nanowires grown vertically on the sapphire substrate have been prepared, and the length and diameter of the nanowires are around 1.5 μm and 30 nm, respectively. Figure 1(b) shows the high-resolution TEM image of an individual ZnO nanowire, and well-defined lattice fringes can be seen from the image. The inset of Fig. 1(b) shows the corresponding Fourier transform pattern of the lattice fringes, from which clear spots can be observed, which indicates that the nanowire is of single crystalline. Figure 1(c) shows the 12 K and 300 K PL spectra of the nanowires. The 12 K spectrum is composed of five peaks at around 3.380, 3.365, 3.323, 3.244, and 3.177 eV. The peak at 3.380 eV can be attributed to the free exciton (FX) emission of ZnO according to its position [29,30]. The dominant FX emission at 12 K symbolizes the high optical quality of the nanowires. The peaks at 3.365 and 3.323 eV have been frequently observed in the PL of ZnO, and they can be attributed to the emission from the neutral donor bound excitons (D^0X) and the transition between the free electrons in the conduction band to the acceptor levels (eA^0) of ZnO, respectively. As for the peaks at 3.244 and 3.177 eV, since their energy difference with eA^0 is 79 and 146 meV, close to the phonon energy of ZnO (72 meV) [30], they can then be attributed to the first and second phonon replica of eA^0, respectively. The PL spectrum at 300 K shows an emission at 3.312 eV, which corresponds to the near-band-edge emission of ZnO [17,30]. The high optical quality of the ZnO nanowires lays a solid ground for the high-performance ZnO-based LEDs employing the nanowires as an active layer. Figure 1(d) shows the XRD pattern of the ZnO nanowires; a single peak at around 34.41° is visible in the pattern, which can be indexed to the diffraction from the (0002) facet of wurtzite ZnO. Note that the shoulder near the peak comes from the diffraction of the (0002) facet under the excitation of Cu Kα2 line. The XRD results indicate that the nanowires are grown along ⟨0001⟩ direction of wurtzite structure.

As stated above, to form *p-n* heterostructures, nitrogen-doped ZnMgO layers have been deposited onto the ZnO nanowires. The Mg content in the ZnMgO layer determined by energy dispersive x-ray spectroscopy (EDS) is 0.32. Since the $Zn_{0.68}Mg_{0.32}O$:N layers were coated onto the conductive ZnO nanowires, a direct Hall measurement on the electrical properties of the $Zn_{0.68}Mg_{0.32}O$:N layer will be interfered greatly by the nanowires. Thus to assess the electrical properties of the $Zn_{0.68}Mg_{0.32}O$:N layers, Hall measurements have been carried out on the layers grown directly on sapphire substrate in the same growth process, which shows that the layers show *p* type conduction with a hole concentration of around 3×10^{16} cm^{-3} and a Hall mobility of 4 cm^2 V^{-1} s^{-1}. We then deduce that the $Zn_{0.68}Mg_{0.32}O$:N layers deposited onto the ZnO nanowires are of *p* type conduction, although the hole concentration and Hall mobility of the layer deposited onto the ZnO nanowires may be slightly different from those of the layer grown directly onto the sapphire substrate. Figures 2(a) and 2(b) show the cross-sectional and plane-view SEM images of the $Zn_{0.68}Mg_{0.32}O$:N coated ZnO nanowires. One can see from the figures that the top surface of the nanowires has been fully covered by the $Zn_{0.68}Mg_{0.32}O$:N. The absorption spectrum of the $Zn_{0.68}Mg_{0.32}O$:N coated ZnO nanowires is shown in Fig. 2(c), from which a sharp peak at around 363 nm can be seen, which comes from the excitonic absorption of the ZnO nanowires. Another absorption edge at around 300 nm also can be observed from the spectrum, which should come from the absorption of the $Zn_{0.68}Mg_{0.32}O$:N layer. The EDS pattern of the $Zn_{0.68}Mg_{0.32}O$:N layer is shown in Fig. 2(d), from which the signals of Mg, Zn,

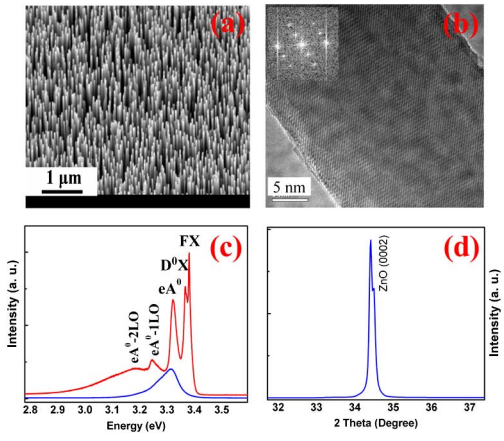

Fig. 1. (a) 30° titled SEM image of the ZnO nanowires grown on sapphire substrate. (b) High-resolution TEM image of an individual ZnO nanowire, and the inset shows the corresponding Fourier transform pattern. (c) 12 K and 300 K PL spectra of the nanowires. (d) XRD pattern of the ZnO nanowires.

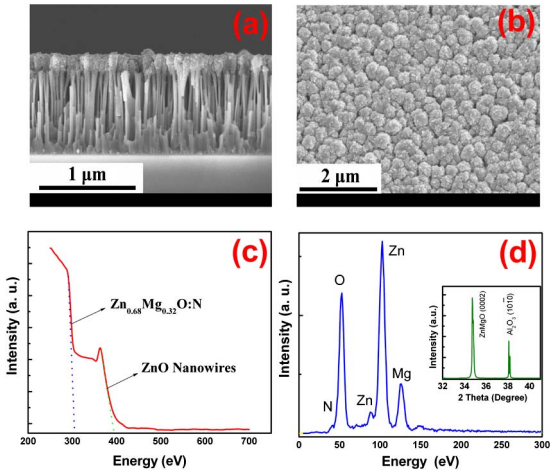

Fig. 2. Cross-sectional (a) and plane-view (b) SEM image of the $Zn_{0.68}Mg_{0.32}O$:N coated ZnO nanowires. (c) The absorption spectrum and energy dispersive x-ray spectroscopy (d) of the $Zn_{0.68}Mg_{0.32}O$:N, and the inset (d) shows the XRD pattern of $Zn_{0.68}Mg_{0.32}O$:N layer.

O, and N can be observed, indicating nitrogen has been incorporated into the $Zn_{0.68}Mg_{0.32}$ layer. The inset of Fig. 2(d) shows the XRD pattern of the $Zn_{0.68}Mg_{0.32}O$:N layer, one sharp peak at around 34.74° and one broad one at around 38.10° can be observed; the former comes from the $Zn_{0.68}Mg_{0.32}O$:N layer, while the latter from the substrate. The XRD results reveal that the $Zn_{0.68}Mg_{0.32}O$:N layer is crystallized in wurtzite structures. One can see in Fig. 2 that the $Zn_{0.68}Mg_{0.32}O$:N layer has the same crystalline structure with ZnO but has a larger bandgap, which provides an ideal arena for constructing heterostructures employing the high structural and optical quality ZnO nanowires as the active layer. When a forward bias is applied onto the heterostructures, holes in the $Zn_{0.68}Mg_{0.32}O$:N layer will be drifted to the ZnO nanowires. While the electrons in the undoped ZnO nanowires will be drifted toward the $Zn_{0.68}Mg_{0.32}O$:N layer and concentrated at the $Zn_{0.68}Mg_{0.32}O$/ZnO interface, as the conduction band offset between these two layers (0.55 eV) will prevent the drifting of electrons from the ZnO nanowires into the $Zn_{0.68}Mg_{0.32}O$:N layer. As a result, electrons and holes will recombine in the ZnO nanowires, and thanks to the relatively high structural and optical quality of the nanowires, high-performance ZnO LEDs may be realized from these heterostructures.

To test the above idea, the luminescence properties of the $Zn_{0.68}Mg_{0.32}O$:N/ZnO nanowire heterostructures have been studied. The inset of Fig. 3 shows the schematic diagram of the heterostructure devices. In these heterostructures, two In dots have been deposited onto the nanowire as a contact, while several Ni/Au bars were evaporated onto the $Zn_{0.68}Mg_{0.32}O$:N layer acting as a contact. The current-voltage (I–V) characteristics of the heterostructures are illustrated in Fig. 3. From the figure, an obvious rectification behavior can be seen, and the turn-on voltage is about 4.2 V. When a positive bias is applied onto the Ni/Au contact, while a negative bias onto the In contact, blue emission can be observed from the heterostructures, as shown in Fig. 4. One can see that when a current of several milliamperes is injected into the device, an emission located at around 390 nm can be detected, while the deep-level related emission at around 500 nm, which has been frequently

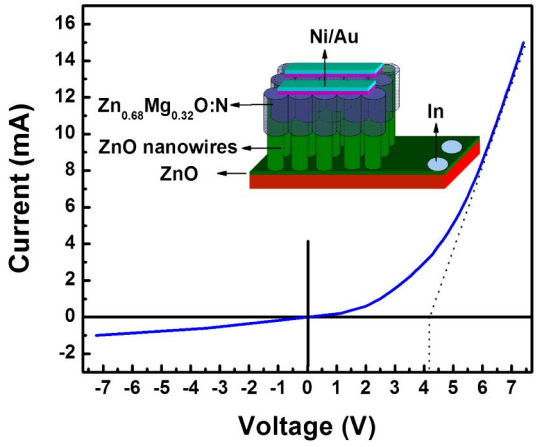

Fig. 3. I–V curve of the $Zn_{0.68}Mg_{0.32}O$:N/ZnO nanowire heterostructures, and the inset shows the schematic diagram of the device.

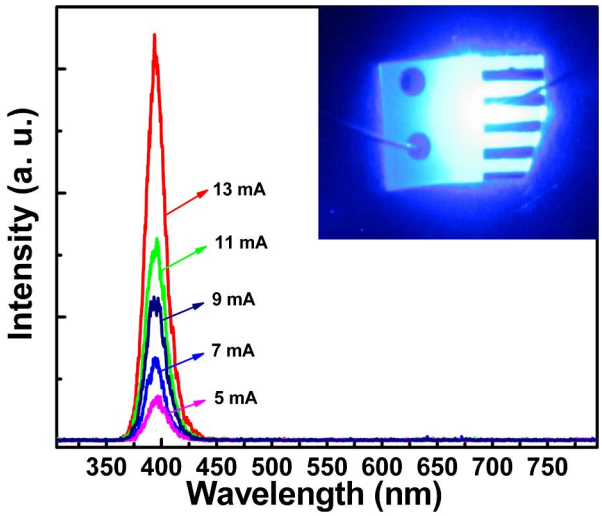

Fig. 4. EL spectra of the device under different injection current, and the inset shows the emission image of the device.

observed in ZnO-based p-n junctions [17,19–22,28], is almost totally invisible. That is, pure UV emission has been obtained from the $Zn_{0.68}Mg_{0.32}O$:N/ZnO nanowire heterostructure LEDs. Note that emission peak shifts little when the injection current increases from 5 to 13 mA (corresponds to a current density from about 125 to 325 mA/cm^2, which is believed to be the combined effect of carrier screening and active layer heating. The inset of this figure shows the emission image of the device; one can clearly observe brilliant blue emissions. Stability is one of the most important parameters for an LED. To test the stability of the device, a current density of 500 mA/cm^2 has been injected into the device continuously, and the emission of the LEDs has been recorded intermediately, as shown in Fig. 5. From the figure, one can find that the device can work continuously for over 27 h, and the emission intensity decreased by around 30% after 27 h, indicating good stability of the device. Note that very few reports demonstrated the continuous operation of ZnO-based LEDs [31–33]; the 27 h reported in this Letter is the longest lifetime ever reported in ZnO-based LEDs. We think the pure UV emission and good stability of the devices are mainly due to the relatively high

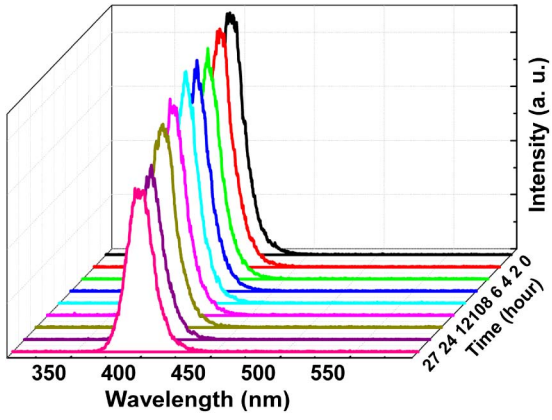

Fig. 5. EL spectra of the device recorded intermediately after continuous running for a while under an injection current density of 500 mA/cm^2.

structural and optical properties of the ZnO nanowires, which act as an active layer in the devices.

In conclusion, well-aligned single-crystalline ZnO nanowires have been prepared, and the nanowires show relatively high structural and optical quality. By employing the nanowires as an active layer, $Zn_{0.68}Mg_{0.32}O$:N/ZnO nanowire heterostructure devices have been fabricated. The devices show pure UV emission when a forward bias is applied, while the frequently observed deep-level emission in ZnO based *p-n* junctions is totally invisible. The device can operate continuously for over 27 h, which is the longest lifetime ever reported in ZnO-based LEDs. The pure UV emission and good stability of the LEDs are believed to be mainly due to the high structural and optical quality of the ZnO nanowires. The results reported in this Letter promise that high-performance ZnO-based LEDs may be achieved.

This work is supported by the National Basic Research Program of China (2011CB302005), the Natural Science Foundation of China (11074248, 11104265, 11374296, and 61177040), and the Science and Technology Developing Project of Jilin Province (20111801).

References

1. E. Matioli, S. Brinkley, K. M. Kelchner, Y. L. Hu, S. J. Nakamura, S. DenBaars, J. Speck, and C. Weisbuch, Light: Sci. Appl. **1**, 22 (2012).
2. G. Y. Zhu, C. X. Xu, L. S. Cai, J. T. Li, Z. L. Shi, Y. Lin, G. F. Chen, T. Ding, Z. S. Tian, and J. Dai, ACS Appl. Mater. Interfaces **4**, 6195 (2012).
3. Y. G. Ma, X. Guo, X. Q. Wu, L. Dai, and L. M. Tong, Adv. Opt. Photon. **5**, 216 (2013).
4. H. X. Dong, Y. Liu, J. Lu, Z. H. Chen, J. Wang, and L. Zhang, J. Mater. Chem. C **1**, 202 (2013).
5. J. Huang, S. Chu, J. Y. Kong, L. Zhang, C. M. Schwarz, G. P. Wang, L. Chernyak, Z. H. Chen, and J. L. Liu, Adv. Opt. Mater. **1**, 179 (2013).
6. G. Lozano, D. J. Louwers, S. R. K. Rodrıguez, S. Murai, O. T. Jansen, M. A. Verschuuren, and J. G. Rivas, Light: Sci. Appl. **2**, 66 (2013).
7. K. W. Wu, P. Ding, Y. F. Lu, X. H. Pan, H. P. He, J. Y. Huang, B. H. Zhao, C. Chen, L. X. Chen, and Z. Z. Ye, Appl. Phys. A **111**, 689 (2013).
8. Q. Qiao, C. X. Shan, J. Zheng, H. Zhu, S. F. Yu, B. H. Li, Y. Jia, and D. Z. Shen, Nanoscale **5**, 513 (2013).
9. X. Y. Liu, C. X. Shan, S. P. Wang, H. F. Zhao, and D. Z. Shen, Nanoscale **5**, 7746 (2013).
10. H. Zhu, C. X. Shan, B. Yao, B. H. Li, J. Y. Zhang, Z. Z. Zhang, D. X. Zhao, D. Z. Shen, X. W. Fan, Y. M. Lu, and Z. K. Tang, Adv. Mater. **21**, 1613 (2009).
11. X. Z. Zhang, X. J. Zhang, J. B. Xu, X. D. Shan, J. Xu, and D. P. Yu, Opt. Lett. **34**, 2533 (2009).
12. M. H. Crawford, IEEE J. Sel. Top. Quantum Electron. **15**, 1028 (2009).
13. N. Tansu, H. P. Zhao, G. Y. Liu, X. H. Li, J. Zhang, H. Tong, and Y. K. Ee, IEEE Photon. J. **2**, 241 (2010).
14. H. P. Zhao, G. Y. Liu, J. Zhang, J. D. Poplawsky, V. Dierolf, and N. Tansu, Opt. Express **19**, A991 (2011).
15. D. F. Feezell, J. S. Speck, S. P. Denbarrs, and S. Nakamura, J. Display Technology **9**, 190 (2013).
16. R. A. Arif, Y. K. Ee, and N. Tansu, Appl. Phys. Lett. **91**, 091110 (2007).
17. F. Sun, C. X. Shan, B. H. Li, Z. Z. Zhang, D. Z. Shen, Z. Y. Zhang, and D. Fan, Opt. Lett. **36**, 499 (2011).
18. K. Nakahara, S. Akasaka, H. Yuji, K. Tamura, T. Fujii, Y. Nishimoto, D. Takamizu, T. Sasaki, H. Tanabe, H. Takasu, T. Amaike, S. F. Onuma, A. Chichibu, A. Tsukazaki, A. Ohtomo, and M. Kawasaki, Appl. Phys. Lett. **97**, 013501 (2010).
19. A. Tsukazaki, T. Onuma, M. Ohtani, T. Makino, M. Sumiya, K. Ohtani, S. F. chichibu, S. Fuke, Y. Segawa, H. Ohno, H. Koinuma, and M. Kawasaki, Nat. Mater. **4**, 42 (2005).
20. A. Tsukazaki, M. Kubota, A. Ohtomo, T. Onuma, K. Ohtani, H. Ohno, S. F. Chichibu, and M. Kawasaki, Jpn. J. Appl. Phys. **44**, L643 (2005).
21. S. J. Jiao, Z. Z. Zhang, Y. M. Lu, D. Z. Shen, B. Yao, J. Y. Zhang, B. H. Li, D. X. Zhao, X. W. Fan, and Z. K. Tang, Appl. Phys. Lett. **88**, 031911 (2006).
22. Z. P. Wei, Y. M. Lu, D. Z. Shen, Z. Z. Zhang, B. Yao, B. H. Li, J. Y. Zhang, D. X. Zhao, X. W. Fan, and Z. K. Tang, Appl. Phys. Lett. **90**, 042113 (2007).
23. X. Huang, L. D. Shao, G. W. She, M. Wang, S. Chen, and X. M. Meng, Cryst. Eng. Comm. **14**, 8330 (2012).
24. Y. Liu, H. X. Dong, S. L. Sun, W. H. Liu, J. X. Zhan, Z. H. Chen, J. Wang, and L. Zhang, Nanoscale **5**, 4123 (2013).
25. H. J. Kim, K. H. Kang, and D. E. Kim, Nanoscale **5**, 6081 (2013).
26. B. O. Jung, Y. H. Kwon, D. J. Seo, D. S. Lee, and H. K. Cho, J. Cryst. Growth **370**, 314 (2013)
27. X. Li, J. J. Qi, Q. Zhang, Q. Wang, F. Yi, Z. Z. Wang, and Y. Zhang, Appl. Phys. Lett. **102**, 221103 (2013)
28. J. S. Liu, C. X. Shan, B. H. Li, Z. Z. Zhang, K. W. Liu, and D. Z. Shen, Opt. Lett. **38**, 2113 (2013).
29. C. X. Shan, Z. Liu, and S. K. Hark, Appl. Phys. Lett. **92**, 073103 (2008).
30. H. B. Zeng, G. T. Duan, Y. Li, S. K. Yang, X. X. Xu, and W. P. Cai, Adv. Funct. Mater. **20**, 561 (2010).
31. J. S. Liu, C. X. Shan, H. Shen, B. H. Li, Z. Z. Zhang, L. Liu, L. G. Zhang, and D. Z. Shen, Appl. Phys. Lett. **101**, 011106 (2012).
32. Z. F. Shi, Y. T. Zhang, J. X. Zhang, H. Wang, B. Wu, X. P. Cai, X. J. Cui, H. W. Liang, B. L. Zhang, and G. T. Du, Appl. Phys. Lett. **103**, 021109 (2013)
33. H. Long, X. M. Mo, H. N. Wang, H. H. Huang, Z. Chen, Y. P. Liu, and G. J. Fang, Appl. Phys. Lett. **103**, 123504 (2013).